The nonlinear association between the Arctic Oscillation and North American winter climate

Aiming Wu[1], William W. Hsieh[1], Amir Shabbar[2]
George J. Boer[3] and Francis W. Zwiers[3]

1 Dept. of Earth and Ocean Sciences, University of British Columbia
Vancouver, BC, Canada, V6T 1Z4
Tel: (604) 822-3932, Fax: (604) 822-6088
E-mail: awu@eos.ubc.ca

2 Climate Research Branch, Meteorological Service of Canada
Downsview, ON, Canada

3 Canadian Center for Climate Modelling and Analysis
Meteorological Service of Canada, University of Victoria
Victoria, BC, Canada

Climate Dynamics

Revised December 2005

Abstract

Nonlinear projections (NLP) of the Arctic Oscillation (AO) index onto North American winter (December–March) 500-mb geopotential height (Z500) and surface air temperature (SAT) anomalies reveal a pronounced asymmetry in the atmospheric patterns associated with positive and negative phases of the AO. In a linear view, the Z500 anomaly field associated with positive AO resembles a positive North Atlantic Oscillation (NAO) pattern with statistically significant positive and negative anomalies stretching zonally into central-eastern USA and Canada respectively, resulting in a cold climate anomaly over northeastern and eastern Canada, Alaska and the west coast of USA, and a warm climate anomaly over the rest of the continent. By contrast, the nonlinear behavior, mainly a quadratic association with AO, which is most apparent when the amplitude of the AO index is large, has the same spatial pattern and sign for both positive and negative values of the index. The nonlinear pattern reveals negative Z500 anomalies over the west coast of USA and the North Atlantic and positive Z500 anomalies at higher latitudes centered over the Gulf of Alaska and northeastern Canada accompanied by cooler than normal climate over the USA and southwestern Canada and warmer than normal climate over other regions of the continent.

A similar analysis is conducted on the data from the Canadian Center for Climate Modelling and Analysis (CCCma) second generation coupled general circulation model (CGCM2). The nonlinear patterns of North American Z500 and SAT anomalies associated with the AO in the model simulation are generally consistent with the observational results, thereby confirming the robustness of the nonlinear behavior of North American winter climate with respect to the AO in a climate simulation that is completely independent of the observations.

1 Introduction

The Arctic Oscillation (AO) was defined by Thompson and Wallace (1998) as the leading empirical orthogonal function (EOF) mode of wintertime sea level pressure (SLP) anomalies over the extratropical Northern Hemisphere. The AO is a seesaw pattern in atmospheric pressure between the Arctic basin and middle latitudes, exhibiting lower than normal pressure over the polar region and higher than normal pressure at mid-latitudes (at about 45°N) in its positive phase, and the reverse in its negative phase. Due to its strong zonal symmetry, the AO is also often referred to as the northern annular mode (NAM; Thompson and Wallace 2000).

Though the climate impacts of the North Atlantic Oscillation (NAO) are largely confined to the sector of the hemisphere extending from eastern Northern America through Europe to central Russia (e.g., Hurrell 1996; Hurrell and van Loon 1997), the impacts of the AO are clearly evident at virtually all longitudes (Thompson and Wallace 2001), including far eastern Asia (e.g. Gong and Ho 2003) and the tropical troposphere (Thompson and Lorenz 2004). Hodges (2000) showed that, in the positive phase of AO, lower than normal atmospheric pressure over the Arctic induces strong westerly winds in the upper atmosphere at northern latitudes, which keep cold Arctic air to the north, leading to a warmer winter in much of the United States (US) east of the Rocky Mountains and central Canada, but leaving Greenland and Newfoundland colder than usual. Meanwhile, with higher than normal atmospheric pressure over the central Atlantic, strong westerly winds push warm and moist air toward northern Europe, leading to wetter weather in Scotland and Scandinavia opposing the drier conditions in the western US and the Mediterranean. In the negative phase of AO, higher than normal atmospheric pressure over the Arctic induces weaker westerly winds in the upper atmosphere, which allow cold Arctic air to reach more southerly latitudes, resulting in a colder winter in the USA but warmer weather in northeastern Canada. Meanwhile, with lower than normal atmospheric pressure in the central Atlantic and weak westerlies over northern Europe, Europe and Asia receive cold Arctic air, and more storms develop over the Mediterranean region. Boer et al. (2001) analyzed the signature of the AO in the momentum and moisture budgets in some depth and provided a schematic of the coupled variation of the components.

The AO also reflects the strength of the stratospheric polar vortex. Stratospheric circulation anomalies can propagate downward to the surface, where they are connected to changes in the magnitude and sign of the AO (Baldwin and Dunkerton 1999, 2001; Baldwin et al. 2003). The AO thus provides a connection between the stratosphere circulation anomalies and the troposphere weather and climate.

The usual assumption is that the atmospheric climate anomalies associated with positive and negative phases of the AO are opposite to each other, i.e., the impact of the AO on the climate is linear. There is, however, some evidence indicating a nonlinear relationship between the AO and northern winter climate. For example, Pozo-Vázquez et al. (2001) found that the winter temperatures in most of Europe do not vary in a linear manner with respect to phase and intensity of the NAO. Similarly, composite anomaly patterns of low AO index winter temperature extremes in the US are considerably different from their counterparts during high AO index winters (Higgins et al. 2002). Shabbar and Bonsal (2004) found a significantly higher frequency of cold spells over eastern Canada, and an increased frequency of winter warm spells over the Canadian Prairies during positive AO winters (relative to negative AO winters). However, the changes in the frequency of the warm spells between positive and negative AO phases are not exactly symmetric to those of the cold spells.

In contrast to the case with the AO, the nonlinear connection of the El Niño–Southern Oscillation (ENSO) with extratropical climate are well documented in recent studies (e.g. Hoerling et al. 1997, 2001; Wu et al. 2003; Wu and Hsieh 2004; Wu et al. 2005). In this study, the nonlinear association between the AO and North American winter climate variation will be examined by a nonlinear projection (NLP) via neural networks (NN). NLP has previously been used to extract the nonlinear atmospheric patterns associated with ENSO (Wu and Hsieh 2004; Wu et al. 2005).

This paper is organized as follows. The data and the NLP method are briefly introduced in Section 2. The nonlinear patterns of the winter 500-mb geopotential height (Z500) and surface air temperature (SAT) anomalies over North America associated with opposite phases of the AO, as extracted by the NLP, are presented in Section 3. A similar analysis but using the data from a 201-year simulation by the Canadian Center for Climate Modelling and Analysis (CCCma) second generation coupled general circulation model (CGCM2) is given in Section 4. Section 5 offers a summary and discussion.

2 Data and methodology

2.1 Observational data

We analyze on a $5°\times5°$ grid the monthly mean of operational Northern Hemispheric SLP analysis as compiled and further extended by Trenberth and Paolino (1980). We consider the period of January 1950 to December 2002, and calculate anomalies by subtracting the monthly climatology based on the whole period (1950-2002) from the data. After weighting the anomalies by the square root of the cosine of the latitude, principal component analysis (PCA, also known as EOF analysis) was performed on winter season anomaly data over the hemisphere from 20°N to the North Pole. Note that we define winter as December–March, while Thompson and Wallace (1998) referred to November–April as the winter season. The standardized leading principal component (PC; accounting for 22.5% of the total variance) is defined as the AO index (Fig. 1c). The loading pattern of the AO is obtained by regressing the gridded SLP anomalies upon the AO index (Fig. 1a) and displays an annular structure over the polar region and two anomaly centers over the North Atlantic and the North Pacific respectively.

The monthly mean Z500 $2.5° \times 2.5°$ gridded data used in this study for the period January 1950 to December 2002 came from the National Center for Environmental Prediction/National Center for Atmospheric Research Reanalysis (Kalnay et al. 1996; downloadable from the National Oceanographic and Atmospheric Administration (NOAA) Climate Diagnostics Center (CDC)). We analyze Z500 variability in the domain [180°–2.5°W, 20°N–90°N], covering the northeastern Pacific, North America and the North Atlantic. In addition, we use a gridded monthly mean land SAT dataset which was obtained from the Climate Research Unit (CRU) at the University of East Anglia, UK (Mitchell et al. 2003, or http://www.cru.uea.ac.uk/cru/data/hrg.htm). This dataset was available on a $0.5° \times 0.5°$ grid for the period 1901–2002. In this study, we use only the data after 1950 and over North America. As with SLP, Z500 and SAT anomalies were calculated by subtracting the 1950-2002 monthly climatology. PCA was then used to compress the gridded anomaly data for the winter season (December–March), retaining the 10 leading Z500 PCs and the 8 leading SAT PCs (accounting for 88.8% and 91.8% of the total Z500 and SAT variance respectively). Experiments show that using more PCs does not alter the final results much.

2.2 Model data

We also use monthly mean SLP, Z500 and SAT data from a 201-year control simulation performed with the CCCma CGCM2 with late 20th century atmospheric concentration of greenhouse gases. A description of the model and its response to increasing greenhouse-gas forcing can be found in Flato and Boer (2001). The data are provided on a 97×48 Gaussian grid (approximately $3.75° \times 3.75°$). Data covering essentially the same domain as in the observational analysis and over the final 100 years of the simulation are used in this study. The standardized leading PC of the winter (December–March) SLP anomalies, which is defined as the model AO index and accounts for 28.1% of the total variance, is shown in Fig. 1d together with the corresponding loading pattern in Fig. 1b. Comparing Figs. 1a and 1b, we see that the spatial structure of the simulated AO is very similar to that of the observations, although the anomaly center over Europe is slightly weaker than observed. As with the observations, the model simulated winter Z500 and SAT anomalies were compressed by PCA with the 10 leading Z500 PCs and the 10 leading SAT PCs (accounting for 90.2% and 71.8% of the total Z500 and SAT variance respectively) retained.

2.3 The NLP model

The NLP technique used in this study employs a multi-layer perceptron NN model with 1-hidden layer (illustrated in the schematic shown in Fig. 2). The NN has a single input, the AO index (x), which is nonlinearly mapped to m intermediate variables called hidden neurons ($h_i, i = 1, \cdots, m$), which are then linearly mapped to l output variables ($y_j, j = 1, \cdots, l$). These output variables are the PCs of either Z500 or SAT. Mathematically, the relationship that links input to output is given by

$$h_i = \tanh(w_i x + b_i), \; i = 1, \cdots, m, \tag{1}$$

$$y_j = \sum_{i=1}^{m} \tilde{w}_{ji} h_i + \tilde{b}_j, \; j = 1, \cdots, l. \tag{2}$$

The characteristics of this statistical model are determined by $m \times (l+1)$ weight parameters ($w_i, i = 1, \cdots, m$, and $\tilde{w}_{ji}, i = 1, \cdots, m, j = 1, \cdots, l$) and $m + l$ bias parameters ($b_i, i = 1, \cdots, m$, and $\tilde{b}_j, j = 1, \cdots, l$). Given enough hidden neurons, this NN model is capable of representing any nonlinear continuous function to arbitrary accuracy (Bishop 1995). Starting from random initial values, the model parameters are optimized so that the mean square error (MSE) between the outputs ($\mathbf{y}$) and the leading PCs of the Z500 (or SAT) anomalies is minimized. There is no time lag between input and output variables. Because the NN model is nonlinear in its parameters, the MSE, when viewed as a function of the parameters, will have multiple local minima. This poses a potential problem when numerical minimization algorithms are used to estimate the parameters. This problem can be avoided by performing the minimization (training) several times starting from randomly chosen initial parameter values, in order to obtain an estimate of the global minimum (Hsieh and Tang 1998). In this study, the NN model was trained 30 times. Among the runs, the solution with the smallest MSE was chosen and the others rejected. To reduce the danger of overfitting by a single NN solution, we repeated the above calculation 400 times with a bootstrap approach (Efron and Tibshirani 1993). A bootstrap sample was obtained by randomly selecting (with replacement) a sample of 53 winters from the original record of 53 winters (for the CGCM2 model data, each bootstrap sample had 100 winters). The ensemble mean of the resulting 400 NN models was used as the final NN model (we averaged the output PCs, not the model parameters). This model was found to be insensitive to the number of hidden neurons, which was varied from 2 to 5 in a sensitivity test. Results from using 3 hidden neurons are presented here.

3 Results from observations

3.1 Composite analysis

Fig. 3 shows composites of the Z500 (and SAT) anomalies for high and low AO-index months. Here low (high) AO-index months refer to the winter months when the value of the AO index is less (larger) than -1.2 (+1.2). Using a lower threshold (e.g. ± 1.0) in choosing composite members did not change the composite anomaly pattern much except for slightly weaker magnitudes and smaller areas of statistical significance at the 5% level. When the AO index is high, the Z500 field (Fig. 3a) has negative anomalies in the north and positive anomalies in the south. The strong anomalies on the eastern side of the domain resemble a positive NAO pattern. Enhanced westerlies over Alaska and northwestern Canada bring warmer maritime air, while anomalous southerlies over the central-eastern US counteract the flow of cold arctic air. The result is warmer than normal temperature over western and south-central Canada and most of the US. The anomalous low pressure centered over Greenland favors the advection of cold air into northeastern and eastern Canada as seen in Fig. 3b. To estimate the statistical significance, composite analysis was performed on each of 400 bootstrap samples, yielding 400 composite anomaly values at each spatial grid. When at least 95% of the values are all positive or all negative, the composite anomaly is considered to be significant at the 5% level at that grid. When the AO index is low, the situation is approximately reversed (Figs. 3c,d)

However, the Z500 and SAT anomaly patterns for low AO-index months are not exactly anti-symmetric to those for high AO-index months, implying a nonlinear association between the AO and North American winter climate. For instance, the Z500 anomaly centers for the high AO composite (Fig. 3a) shows an eastward shift relative to the anomaly centers for the low AO composite (Fig. 3c). This is especially the case for the center positioned over the subtropical North Atlantic.

As a simple estimate of the nonlinear component of the Z500 (or SAT) aspect of the AO, we plot in Figs. 3e and 3f respectively the sum of the Z500 and SAT composites for high and low AO months. The "residual" Z500 anomalies and the implied flow are again consistent with the "residual" SAT anomalies. Note that the significant areas in Figs. 3e,f are much smaller than in Figs. 3a-d, suggesting that the overall impact of AO is mainly linear, esp. over eastern North America and North Atlantic, while over some areas (e.g., the Pacific West Coast), the nonlinear component may be more important.

Although composite analysis is capable of representing the asymmetric (or nonlinear) atmospheric patterns associated with the opposite phases of the AO, such an analysis does not give a continuous nonlinear function connecting the AO index and Z500 and SAT anomalies. For this purpose, we turn to the NLP approach.

3.2 The NLP results

a. Z500

The NN approach connects the AO index time series to a set of, in our case, 10 output PCs of Z500. Weak nonlinearity can be seen between the AO index (x) and the output Z500 PCs from the NLP (not shown). The Z500 atmospheric behavior extracted by the NLP can also be represented as a curve in the 10 dimensional phase space of the Z500 PCs, while the linear projection is a straight line in the same 10-D space. The parabolic nature of this curve when projected onto, for example, the PC_1-PC_2 plane or the PC_2-PC_3 plane (Fig. 4), indicates that the AO index connects nonlinearly to a combination of leading Z500 PCA modes.

To ensure that the nonlinearity detected is not a false positive from the nonlinear method itself, extra NLP experiments were performed from the AO index onto a set of synthetic data, which consist of the linear signal (i.e., the linear regressions of the Z500 PCs on the AO index) and Gaussian noise. The amplitude of the noise was chosen so that the new data had the same mean and standard deviation as the original PCs. Based on 400 sets of such experiments, the NLP did not detect significant nonlinearity from this known linear system.

For a particular value of the AO index, the NN solution predicts the 10 Z500 PCs that are most closely associated with that value. These can be combined with the corresponding EOFs, yielding the Z500 spatial anomalies associated with the given value of the AO index. The atmospheric structure associated with the AO evolves smoothly as the AO index moves along the curve in the PC phase space. In this nonlinear evolution, both the spatial pattern and amplitude change; by contrast to the linear evolution along a straight line in the PC phase space, which results in an evolving amplitude of a fixed spatial pattern.

As the AO takes on its minimum and maximum values, the Z500 anomalies derived from the NLP (in Figs. 5a,b) closely resemble the composite Z500 anomalies of Figs. 3c and 3a in spatial pattern, but have enhanced magnitudes. The asymmetric Z500 anomaly patterns are again apparent in association with low and high AO index. Figs. 5c and 5d show respectively the Z500 anomalies when the AO index takes on half its minimum value and half its maximum value. The Z500 anomalies decrease in magnitude, but are more similar in pattern in Figs. 5c and 5d compared to Figs. 5a and 5b, suggesting that at these half-minimum and half-maximum AO values, the Z500 behavior is nearly linear. In Fig. 5, the shaded areas indicate that, among the results from the 400 bootstrap samples, at least 95% of them are all positive or all negative.

The Z500 anomalies associated with the AO extracted by the NN model can be decomposed into linear and nonlinear components. The linear component is obtained by linear regression of the AO index onto the Z500 field reconstructed from the 10 leading EOF modes of the original Z500 anomalies. The nonlinear component is the residual that remains after subtracting the linear component. The standardized leading PC of the nonlinear component (for the winter months from January 1950 to December 2002) and the corresponding loading pattern are shown in Fig. 6a (dashed line) and Fig. 6c respectively. Since the Z500 anomaly field extracted by the NLP was generated by mapping from a single AO index time series, the first PCA mode accounts for over 99% of the variance of the nonlinear component. When the AO index (shown as the solid line in Fig. 6a) takes on a positive value (+1), the linear component (Fig. 6b) has strong negative anomalies over Greenland and northeastern Canada, and positive anomalies over central-eastern America, North Atlantic and Europe, resembling a positive NAO, while the anomalies over the west are much weaker. When the PC_1 of the nonlinear component takes on a positive value (+1), the Z500 field (Fig. 6c) has positive anomalies stretching from Greenland through Canada to the northeastern Pacific centered over the Gulf of Alaska and the Baffin Island respectively, and negative anomalies extending from subtropical eastern Pacific through US and southern Canada to the North Atlantic. The statistical significance (at the 5% level) of the regression coefficients in Figs. 6b,c is based on a F-test (Weisberg 1985), using 51 degrees of freedom. Note that the anomaly pattern shown in Fig. 6c is basically consistent with the results from the composite analysis (Fig. 3e).

Relative to the linear component (Fig. 6b), the Z500 anomalies of the nonlinear component (Fig. 6c) are much weaker in the eastern region but are comparable or even stronger in the west. Thus the linear component dominates in the Atlantic sector, but the nonlinear component dominates in the Pacific-West Coast area. This is similar to the extratropical effects of ENSO, where the association over the Pacific-North America area is mainly linear, but becomes increasingly nonlinear in the Euro-Atlantic sector (Wu and Hsieh 2004). Furthermore, in Fig. 6a, the maximum magnitude of the dashed curve (for the nonlinear component) is about double that of the solid curve (linear component), thereby considerably amplifying the nonlinear pattern (Fig. 6c) relative to the linear pattern (Fig. 6b).

The PC_1 of the nonlinear component was fitted by least squares to a polynomial of the AO index, where the quadratic term was found to be overwhelmingly dominant (not shown), indicating that the nonlinear connection between North American Z500 and the AO is mainly quadratic. Thus the PC_1 of the nonlinear component (the dashed line in Fig. 6a) has positive values not only during the winters with positive AO index (e.g. 1957, 1959, 1962, 1989, 1990, 1993 and 1997), but also during the winters with negative AO index (e.g. 1958, 1962, 1963, 1966, 1969, 1977 and 1985). Hence, regardless of the sign of the AO index, the nonlinear Z500 component has the same anomaly pattern, namely that of

Fig. 6c.

b. SAT

In a similar way, the SAT anomalies associated with the AO and extracted by the NLP are manifested as a curve in the 8-D phase space of the SAT PCs, which again is parabola-like (not shown), indicating appreciable nonlinearity. When the AO index takes on its minimum value, statistically significant positive temperature anomalies appear over Alaska, northeastern and eastern Canada, and negative anomalies over the rest of the continent centered over the Great Plains (Fig. 7a). When the AO index takes on its maximum value, significant negative anomalies appear over western US, northeastern and eastern Canada, and positive anomalies over the rest of the domain centered over northwestern Canada and eastern US (Fig. 7b). The anomaly pattern shown in Fig. 7a agrees well with the result from composite analysis (Fig. 3d), while the anomaly pattern shown in Fig. 7b is quite different from the composite result (Fig. 3b), i.e., the NLP reveals more asymmetry (nonlinearity) in the SAT field associated with extreme low and high AO index. The SAT anomalies associated with the half minimum AO index and half maximum AO index are shown in Figs. 7c and 7d, respectively, with both the magnitudes of the anomalies and the asymmetry (between the two panels) reduced.

The linear and nonlinear components of the SAT anomalies associated with the AO are obtained in the same way as for the Z500 data. When the AO index (the solid line in Fig. 8a) takes on a positive value, the linear component (Fig. 8b) has significant negative temperature anomalies over northeastern and eastern Canada, and Alaska, and mainly positive anomalies over the rest of the continent centered over the Great Plains. When the PC_1 of the nonlinear component (the dashed line in Fig. 8a) takes on a positive value, the SAT (Fig. 8c) has negative anomalies over the US and southwestern Canada, and positive anomalies over the rest of the continent centered over northeastern Canada and Alaska. Relative to the linear component (Fig. 8b), the nonlinear component (Fig. 8c) is much weaker over the northeast of the continent, but is about 1/2 the magnitude of the linear component in the Great Plains. Again the dashed curve in Fig. 8a has a maximum magnitude about double that of the solid curve.

As was the case for Z500, the time series denoted by the dashed line (Fig. 8a) has positive values not only during the winters with positive AO index but also during the winters with negative AO index, i.e., regardless of the sign of the AO index, the nonlinear SAT component has the pattern depicted in Fig. 8c. The PC_1 of the nonlinear SAT component again can be fitted by a polynomial function of the AO index (not shown), which indicated that the nonlinear relationship between North American winter SAT and the AO is again essentially quadratic.

Both the linear and nonlinear patterns of SAT are linked to the corresponding circulation anomalies. In an obvious way, comparing Figs. 6b and 6c with Figs. 8b and 8c shows anomalous warm (cold) condition when geostrophic Z500 anomalous flow has a component for the north (south).

c. Comparison with the ENSO impacts

Fig. 9 shows the nonlinear Z500 and SAT anomaly pattern associated with ENSO extracted by the NLP (corresponding to Figs. 6c and 8c, respectively in this study). As addressed by Wu and Hsieh (2004) and Wu et al. (2005), regardless of the sign of the ENSO index, the nonlinear Z500 component has negative anomalies over the west coast of North America and Greenland, and positive anomalies extending eastward from central-eastern North America to western Europe (Fig. 9a), resulting in positive SAT anomalies over the US and south-central Canada, and negative SAT anomalies over the rest of the continent (Fig. 9b). Very roughly, the Z500 anomalies in Fig. 9a show a similar spatial pattern but of opposite sign to that in Fig. 6c, except that the positive anomalies over the central-eastern North America extend to higher latitudes in Fig. 9a than the negative anomalies in Fig. 6c. It is not surprising to see that the SAT anomalies in Fig. 9b are approximately opposite to those in

Fig. 8c, but with the positive anomalies centered further east (around the Great Lakes). Thus the AO and ENSO appear to have comparable but opposite nonlinear behaviors in the North American winter climate. For both ENSO and AO, the nonlinear component manifests farther from the source than the linear component. For ENSO and AO, the linear component dominates the Pacific-North America and the Atlantic sector respectively, while the nonlinear component is clearly apparent in the Euro-Atlantic sector for ENSO and the Pacific-West Coast area for AO.

4 Results from the coupled GCM

To further understand the nonlinear aspects of the AO and North America climate variability, similar analysis were performed by using the model data generated by the CCCma CGCM2.

4.1 Composite analysis

Fig. 10a shows that when the model AO index is high, the simulated Z500 field has positive anomalies in the south and negative anomalies in the north of the domain, with stronger anomalies appearing in the east resembling the positive NAO pattern, basically agreeing with the observations (Figs. 3a) except for the slightly weaker magnitudes. Fig. 10c shows similarly good agreement with observation (Fig. 3c) when the AO index is low. The eastward shift of the positive anomaly center over the subtropical North Atlantic in Fig. 10a relative to its counterpart in Fig. 10c is also well simulated by the model, indicating some nonlinearity in the Z500 association field. The main discrepancy is found between the model simulation and observations over the northeastern Pacific and southern Alaska during high AO-index episodes, where the observations reveal positive anomalies (Fig. 3a), while the model gives negative anomalies (Fig. 10a), which are nearly in anti-symmetry to the anomalies during low AO-index episodes (Fig. 10c), suggesting that the model underestimates the nonlinearity in the

Z500 field in this region. The sum of the Z500 high and low AO composites in Figs. 10a and 10c is an indication of the nonlinear component as shown in Fig. 10e. The spatial pattern is roughly similar to the observational result (Fig. 3e) except that statistically significant anomalies are largely confined over northeastern Canada and subtropical North Atlantic.

The SAT composite for low AO-index months shows positive anomalies over Alaska, northeastern Canada, Labrador, Newfoundland and western Mexico, and negative anomalies over the rest of the continent (Fig. 10d). Despite the similarity in the spatial pattern, the composite SAT for high AO-index months (Fig. 10b) is not exactly anti-symmetric to that for low AO-index months. The model SAT anomaly patterns are broadly similar to those of the observations (Figs. 3b,d) although there are some discrepancies in location and magnitude. The sum of the SAT anomalies in Figs. 10b and 10d reveals positive anomalies over northern and northeastern Canada, southwestern US and western Alaska, which are in contrast to the negative anomalies over other parts of the continent (Fig. 10f), broadly in agreement with the observations (Fig. 3f).

4.2 The NLP results

a. Z500

The Z500 anomalies extracted by the NLP associated with minimum and maximum AO index values (as shown in Figs. 11a and 11b, respectively) closely resemble the composite results but with considerably enhanced magnitudes. Comparing Fig. 11a with 11b, we see again weak asymmetry of the circulation anomalies in the west, and the displacement of anomaly centers in the east (particularly over the North Atlantic). Also, the Z500 anomalies associated with half minimum and maximum AO index values show very similar spatial patterns (Figs. 11c,d).

The linear and nonlinear components of the Z500 variability were separated as before. When the model's AO index (shown as the solid line in Fig. 12a) takes on positive values, the linear pattern (Fig. 12b) generally agrees well with the observations (Fig. 6b) although magnitudes are somewhat weaker and the trough over the Gulf of Alaska is somewhat more prominent. When the PC_1 of the nonlinear component (the dashed line in Fig. 12a) takes on positive values, the spatial pattern (Fig. 12c) roughly agrees with the observations (Fig. 6c) although the model underestimates the ridge in the west. Again, the time series denoted by the dashed line in Fig. 12a has positive values not only during winter with large positive AO index but also during winter with large negative AO index. That is, regardless of the sign of the AO index, the Z500 has the same anomaly pattern as depicted by Fig. 12c.

b. SAT

The SAT anomalies derived from the NLP associated with minimum, and maximum AO index values (as shown in Figs. 13a and 13b respectively) agree with the results from the composite analysis (Figs. 10d and 10b) but with enhanced magnitudes, showing some asymmetry in the SAT anomaly field during extreme opposite phases of the AO, while the SAT anomalies associated with half minimum and maximum AO index values are nearly anti-symmetric (Figs. 13c,d). This behavior is similar to that for the observations in Fig. 7.

When the AO index takes on a positive value, the linear component (Fig. 14b) agrees reasonably well with the observational result (Fig. 8b). When the PC_1 of the nonlinear component takes on a positive value, the SAT field (Fig. 14c) also agrees with the observational result (Fig. 8c) although magnitudes are somewhat weaker and the pattern is displaced slightly northward.

5 Summary and discussion

Nonlinear aspects of the AO and North American winter climate are investigated by a nonlinear projection via neural networks. Both composite analysis and the NLP yield similar anomaly patterns for Z500 and SAT that exhibit considerable asymmetry during the opposite phases of the AO, showing a nonlinear association between the AO and North American winter climate variability. The Z500 and SAT anomalies associated with the AO, as extracted by the NLP, were decomposed into linear and nonlinear components. The nonlinear component behavior is fundamentally different from that of the linear component in that its magnitude varies with that of the linear component but its sign does not (i.e., there is a quadratic relationship). Thus the same nonlinear component modulates both the positive and negative linear component patterns. It is an outstanding problem to understand how the essentially quadratic nature of the nonlinear behavior follows from the structure of the governing equations.

It is interesting to find that the AO and ENSO appear to have comparable but approximately opposite nonlinear behavior in North American winter climate. For ENSO behavior, the linear component is largely confined in the Pacific-North America area, while the nonlinear component is manifested clearly in the Euro-Atlantic sector. For the AO behavior, the linear component is dominant in the Atlantic sector, while the nonlinear component becomes increasingly important in the Pacific-West Coast area. In other word, for both ENSO and AO, the nonlinear behavior manifests a "teleconnection" at a greater distance from the source than the linear component. Though the physical mechanism for this nonlinear teleconnection is not clear so far, making use of this nonlinear information may potentially contribute additional seasonal climate prediction skill. We found that cross-validated correlation and root mean square error (RMSE) skills for both Z500 and SAT can be improved by using the quadratic term of the AO index as an additional predictor (not shown).

The robustness of the nonlinear association between the AO and North America climate found in the observational data is further investigated in the results of the CCCma CGCM2 coupled climate model. Although there are some differences, the nonlinear patterns of North American Z500 and SAT anomalies associated with the AO generated in the model basically agree with the observational results, strongly suggesting that the nonlinear behavior of North American winter climate with respect to the AO is real as this phenomenon is found in observations and in a climate simulation that is completely independent of the observations. This similarity between model simulation and observations also increases our confidence in the climate model.

Acknowledgements

This study was supported by a strategic grant from the Natural Sciences and Engineering Research Council of Canada, and a contribution from Environment Canada. Dr. David Viner of the Climatic Research Unit at the University of East Anglia kindly provided the surface air temperature data. We are also grateful for the computational resources from Westgrid.

References

Baldwin MP, Dunkerton TJ (1999) Propagation of the Arctic Oscillation from the stratosphere to the troposphere. J Geophys Res 104: 30937-30946

Baldwin MP, Dunkerton TJ (2001) Stratospheric harbingers of anomalous weather regimes. Science 294: 581-584

Baldwin MP, Stephenson DB, Thompson DWJ, Dunkerton TJ, Charlton AJ, O'Neill A (2003) Stratospheric memory and extended-range weather forecasts. Science 301: 636-640

Bishop CM (1995) *Neural networks for pattern recognition.* Clarendon Pr. Oxford.

Boer GJ, Fourest S, Yu B (2001) The signature of the annular modes in the moisture budget. J Clim 14: 3655-3665

Efron B, Tibshirani RJ (1993) *An Introduction to the Bootstrap*, CRC, Boca Raton.

Flato GM, Boer GJ (2001) Warming asymmetry in climate change simulations. Geophys Res Lett 28: 195-198

Gong D, Ho C (2003) Arctic oscillation signals in the East Asian summer monsoon. J Geophys Res 108: 4066, doi:10.1029/2002JD002193

Higgins RW, Leetmaa A, Kousky VE (2002) Relationships between climate variability and winter temperature extremes in the United States. J Clim 15: 1555-1572

Hodges G (2000) The new cold war. Stalking arctic climate change by submarine. *National Geographic*, March, 30-41

Hoerling MP, Kumar A, Zhong M (1997) El Niño, La Niña and the nonlinearity of their teleconnections. J Clim 10: 1769-1786

Hoerling MP, Kumar A, Xu T (2001) Robustness of the nonlinear climate response to ENSO's extreme phases. J Clim 14: 1277-1293

Hsieh WW, Tang B (1998) Applying neural network models to prediction and data analysis in meteorology and oceanography. Bull Amer Meteor Soc 79: 1855-1870

Hurrell JW (1996) Influence of variations in extratropical wintertime teleconnections on Northern Hemisphere temperature. Geophys Res Lett 23: 665-668

Hurrell JW, van Loon H (1997) Decadal variations in climate associated with the North Atlantic Oscillation. Climate Change 36: 301-326

Kalnay ME et al (1996) The NCEP/NCAR Reanalysis Project. Bull Amer Meteor Soc 77: 437-471

Mitchell TD, Carter TR, Jones PD, Hulme M, New M (2003) A comprehensive set of high-resolution grids of monthly climate for Europe and the globe: the observed record (1901-2000) and 16 scenarios (2001-2100). J Clim (submitted)

Pozo-V*á*zquez D, Esteban-Parra MJ, Rodrigo FS, Castro-Diez Y (2001) A study of NAO variability and its possible nonlinear influences on European surface temperature. Clim Dyn 17: 701-715

Shabbar A, Bonsal B (2004) Associations between low frequency variability modes and winter temperature extremes in Canada. Atmos.-Ocean 42: 127-140

Thompson DWJ, Wallace JM (1998) The Arctic Oscillation signature in the wintertime geopotential height and temperature fields. Geophy Res Lett 25: 1297-1300

Thompson DWJ, Wallace JM (2000) Annular modes in the extratropical circulation. Part 1: Month-to-month variability. J Clim 13: 1000-1016

Thompson DWJ, Wallace JM (2001) Regional climate impacts of the Northern Hemisphere annular mode. Science 293: 85-89

Thompson DWJ, Lorenz DJ (2004) The signature of the annular modes in the tropical troposphere. J Clim 17: 4330-4342

Trenberth KE, Paolino DA (1980) The Northern Hemisphere sea level pressure data set: Trends, errors and discontinuities. Mon Wea Rev 108: 855-872

Weisberg S (1985) Applied linear regression (Second Edition). A Volume in the Wiley Series in Probability and Mathematical Statistics: Barnett V et al Ed. pp 17-18

Wu A, Hsieh WW, Zwiers F (2003) Nonlinear modes of North American winter climate variability derived from a general circulation model simulation. J Clim 15: 2325-2339

Wu A, Hsieh WW (2004) The nonlinear Northern Hemisphere winter atmospheric response to ENSO. Geophys Res Lett 31: L02203, DOI:10.1029/2003GL018885

Wu A, Hsieh WW, Shabbar A (2005) The nonlinear patterns of North American winter temperature and precipitation associated with ENSO. J Clim 1736-1752

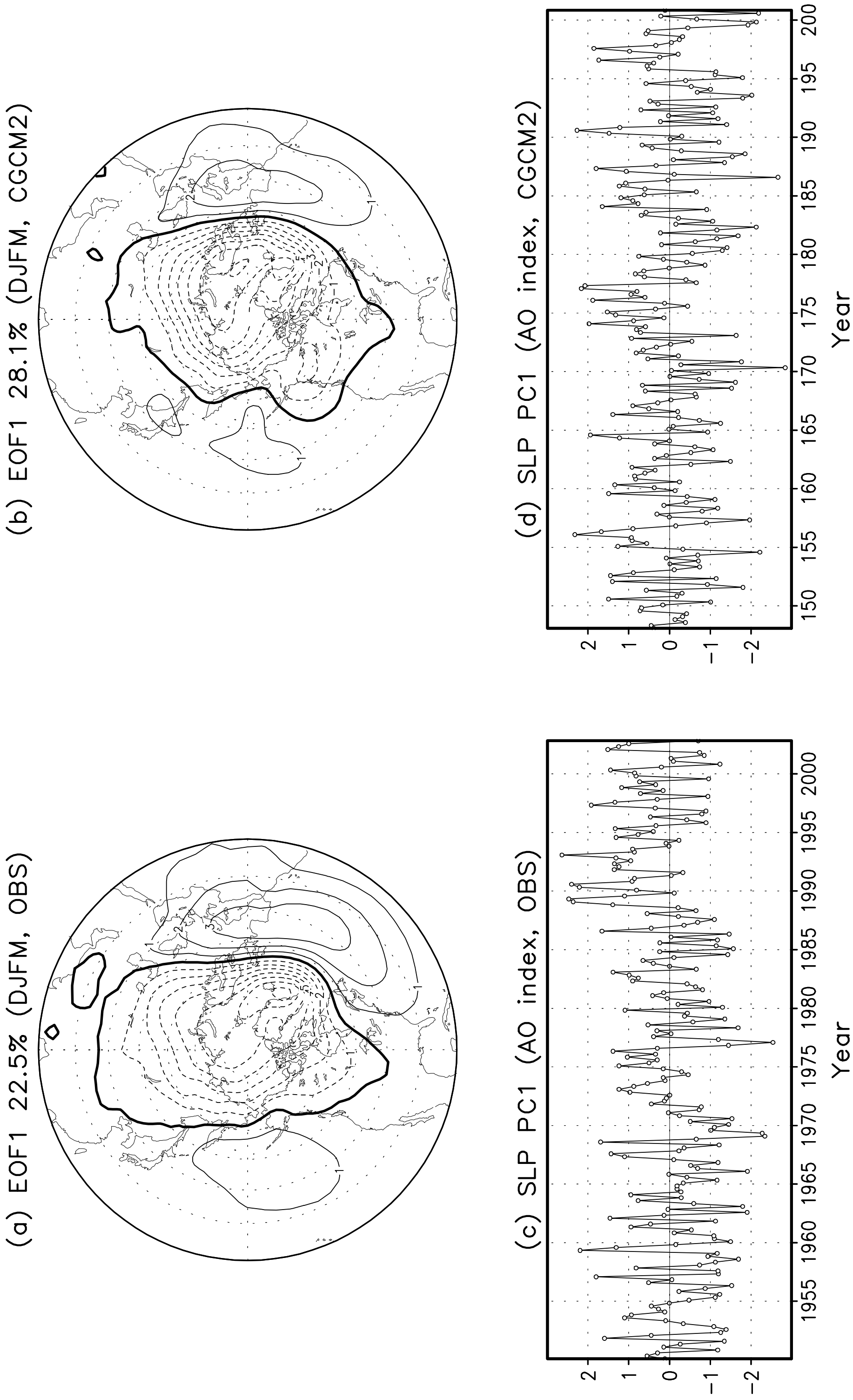

Figure 1: The leading empirical orthogonal function (EOF) of Northern Hemispheric winter (December–March) SLP anomalies and the corresponding principal component (PC). The standardized PC is defined as the AO index. Panels (a) and (c) present results based on observations, while panels (b) and (d) are from the CCCma CGCM2. In panels (a) and (b), solid curves denote positive contours, dashed curves, negative contours, and thick curves, the zero contours. The contour interval is 1 hPa.

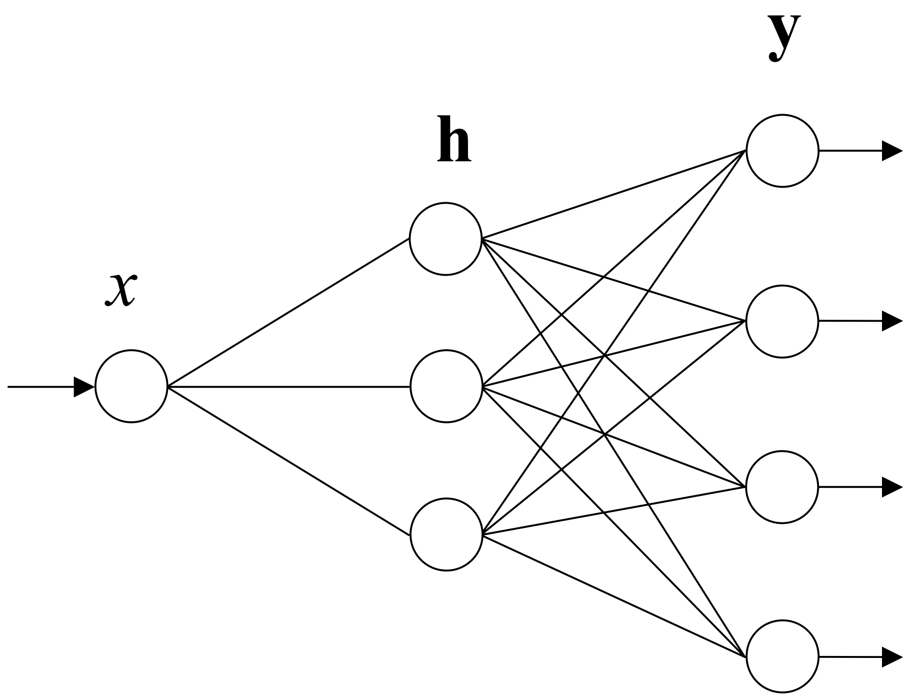

Figure 2: A schematic diagram of the feed-forward neural network (NN) model used to perform the nonlinear projection. The single input x is mapped forward to intermediate variables (hidden neurons) h_i, which are in turn mapped to the output variables y_j.

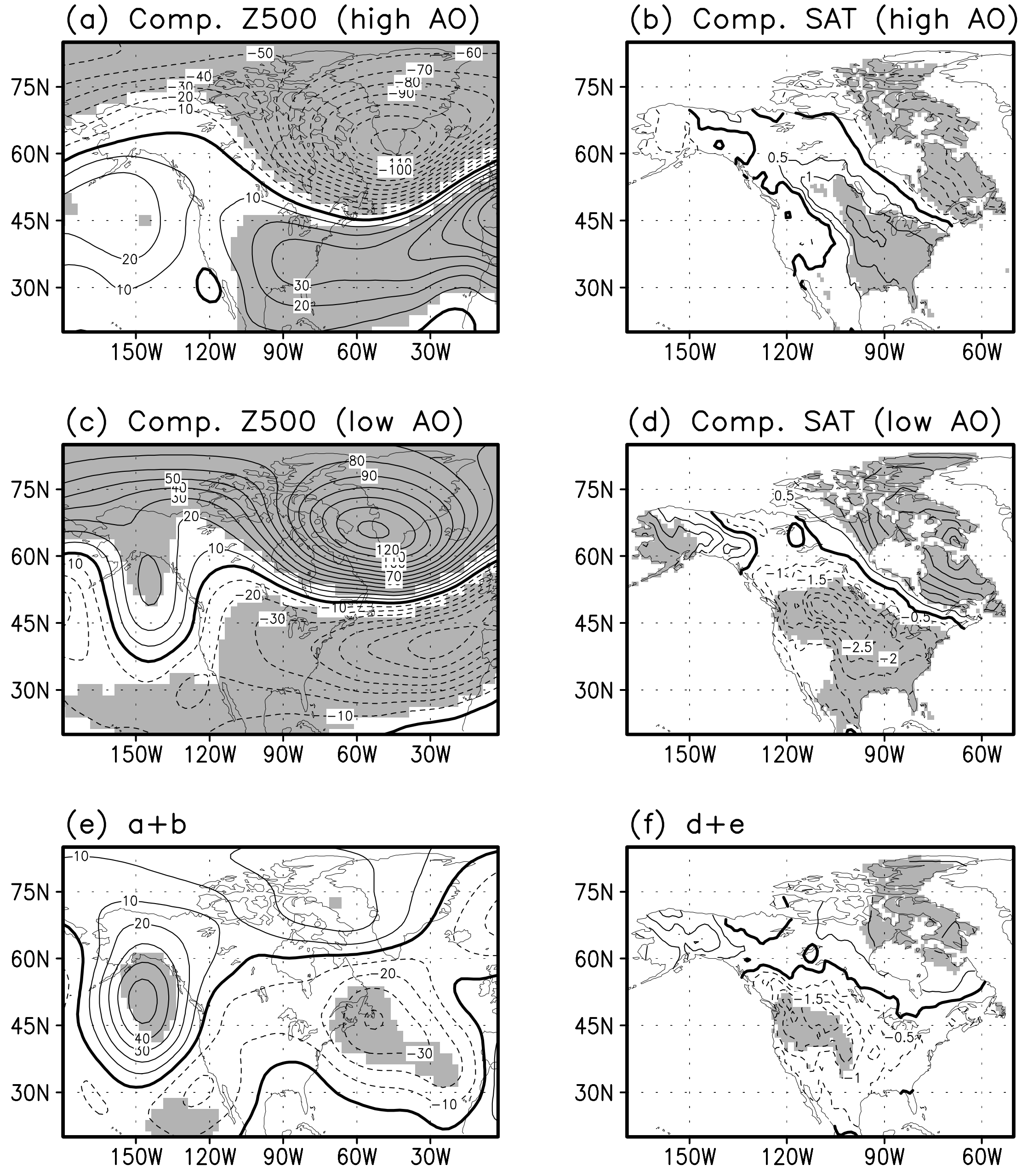

Figure 3: Composite maps of the Z500 anomalies (a) for high AO-index winter months, and (c) for low AO-index winter months. The sum of the anomalies in panel (a) and those in panel (c) is shown in panel (e) to present the nonlinear component of the Z500 anomalies associated with the AO. Similarly, panels (b), (d) and (f) show the results of the SAT field. The contour interval is 10m for the Z500 field (left column), and 0.5°C for the SAT field (right column). The gray areas are where the anomalies are statistically significant at the 5% level from bootstrapping.

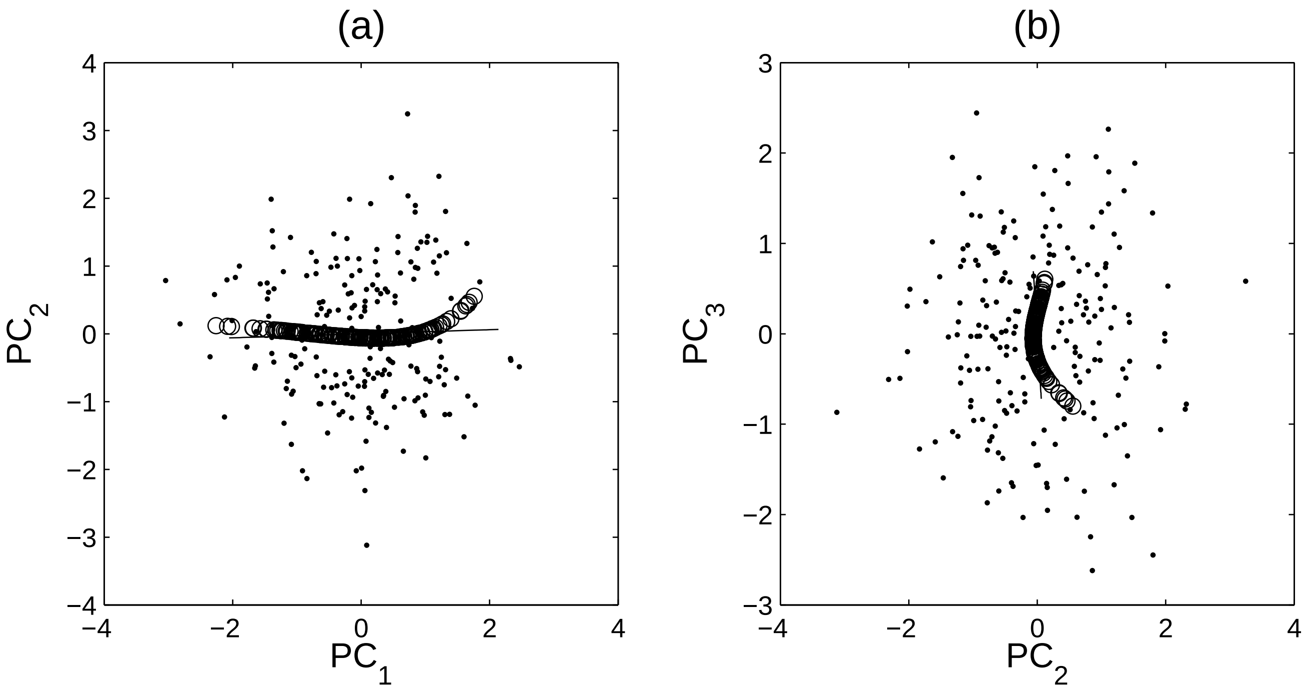

Figure 4: The NLP results of projected onto (a) the Z500 PC_1-PC_2, and (b) PC_2-PC_3 planes, as shown by the curve with overlapped circles, compared to the linear projection, the straight line. The original data (normalized) are shown with the scattered dots.

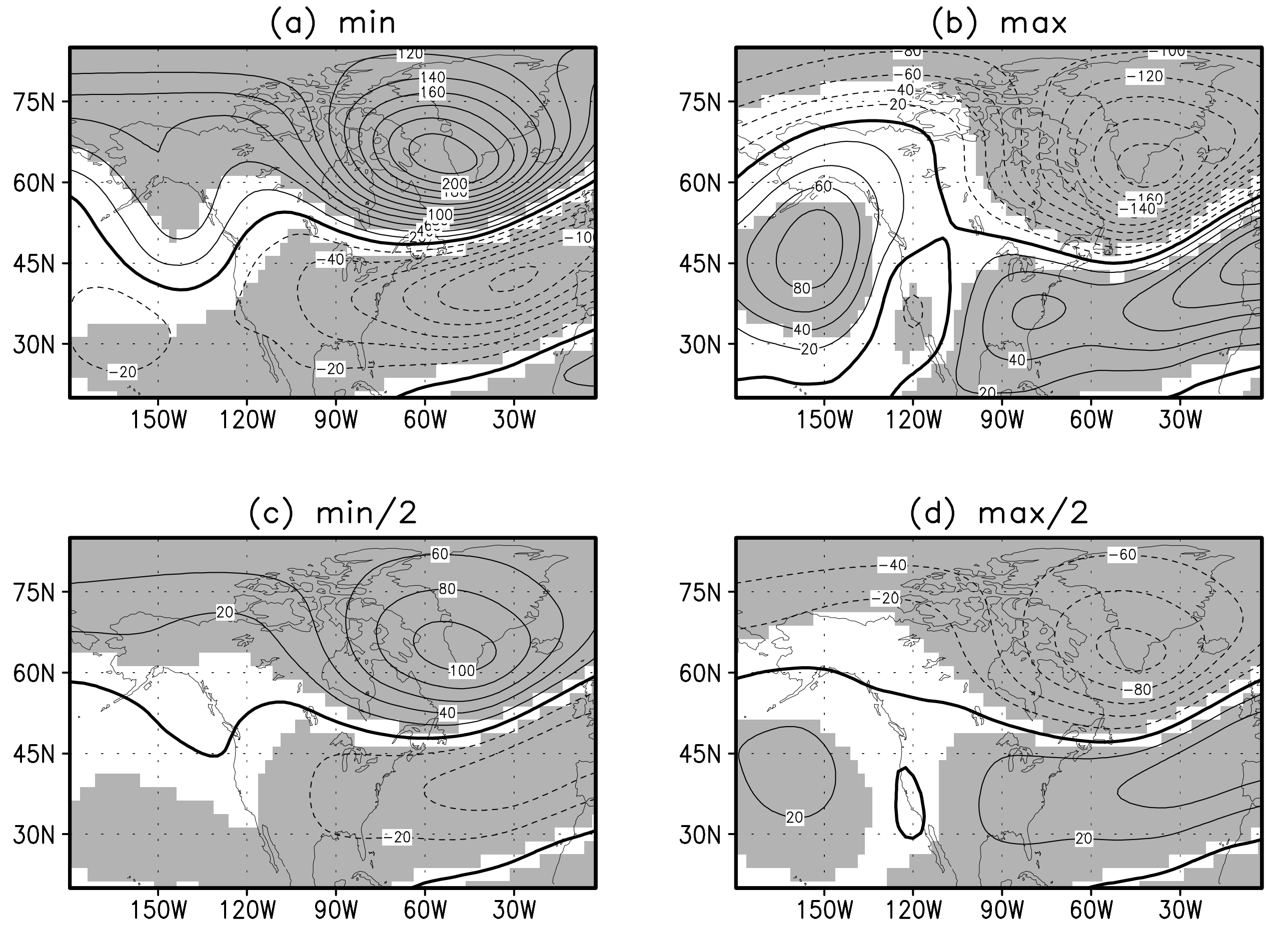

Figure 5: The Z500 anomalies extracted by the NLP associated with (a) minimum AO index, (b) maximum AO index, (c) one half of the minimum AO index, and (d) one half of the maximum AO index. Contour interval is 20m and the grey areas indicate statistical significance at the 5% level, based on the distribution of the results from the 400 bootstrap samples.

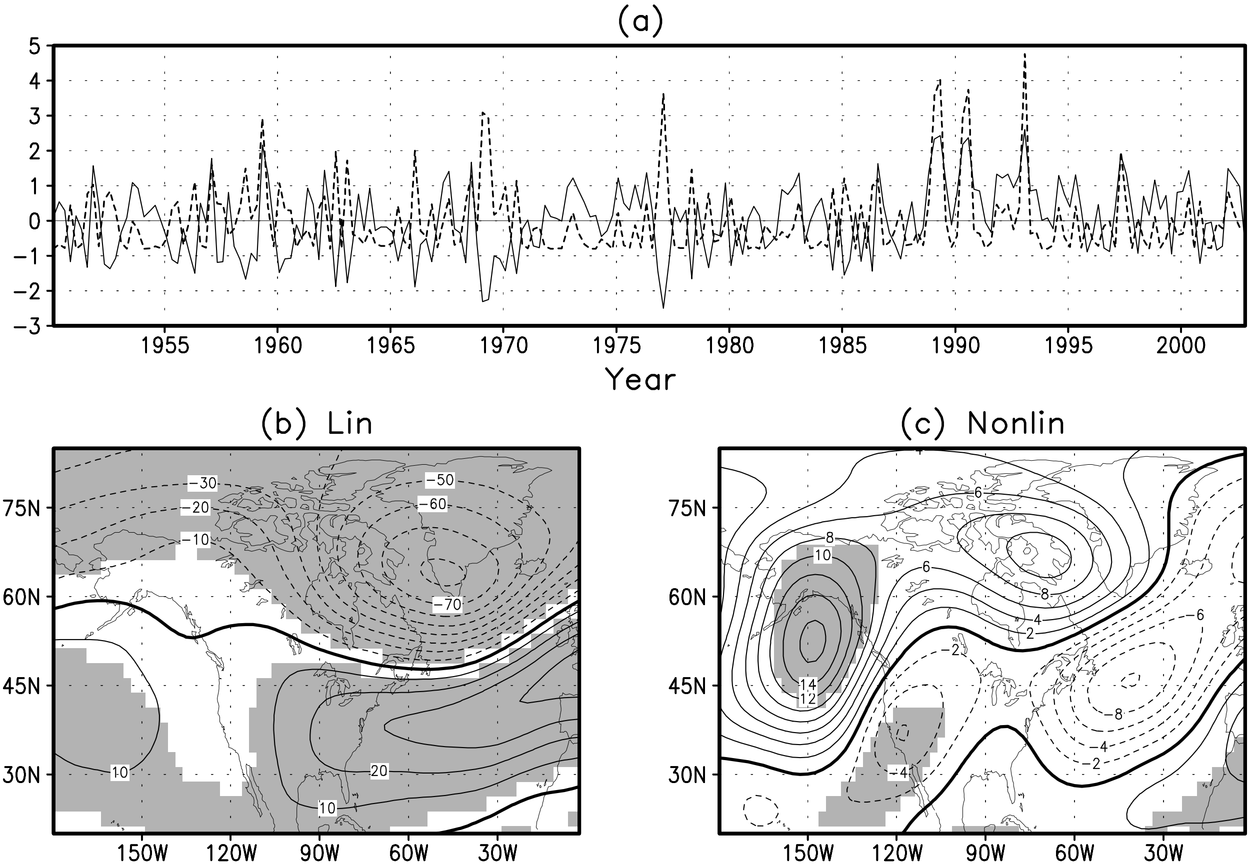

Figure 6: The standardized leading PC of the nonlinear component of the Z500 anomalies associated with the AO as extracted by the NLP, shown by the dashed line in panel (a). The AO index is also shown (as the solid line) for comparison. Tick marks along the abscissa indicate January of the year. Regressing the Z500 anomalies upon the AO index yields the linear pattern (b); while regressing the Z500 anomalies upon the time series denoted by the dashed line in panel (a) yields the pattern for nonlinear component (c). The contour interval is 10m in panel (b), and 2m in panel (c). The regression coefficients are statistically significant at the 5% level in the gray areas (based on a F-test).

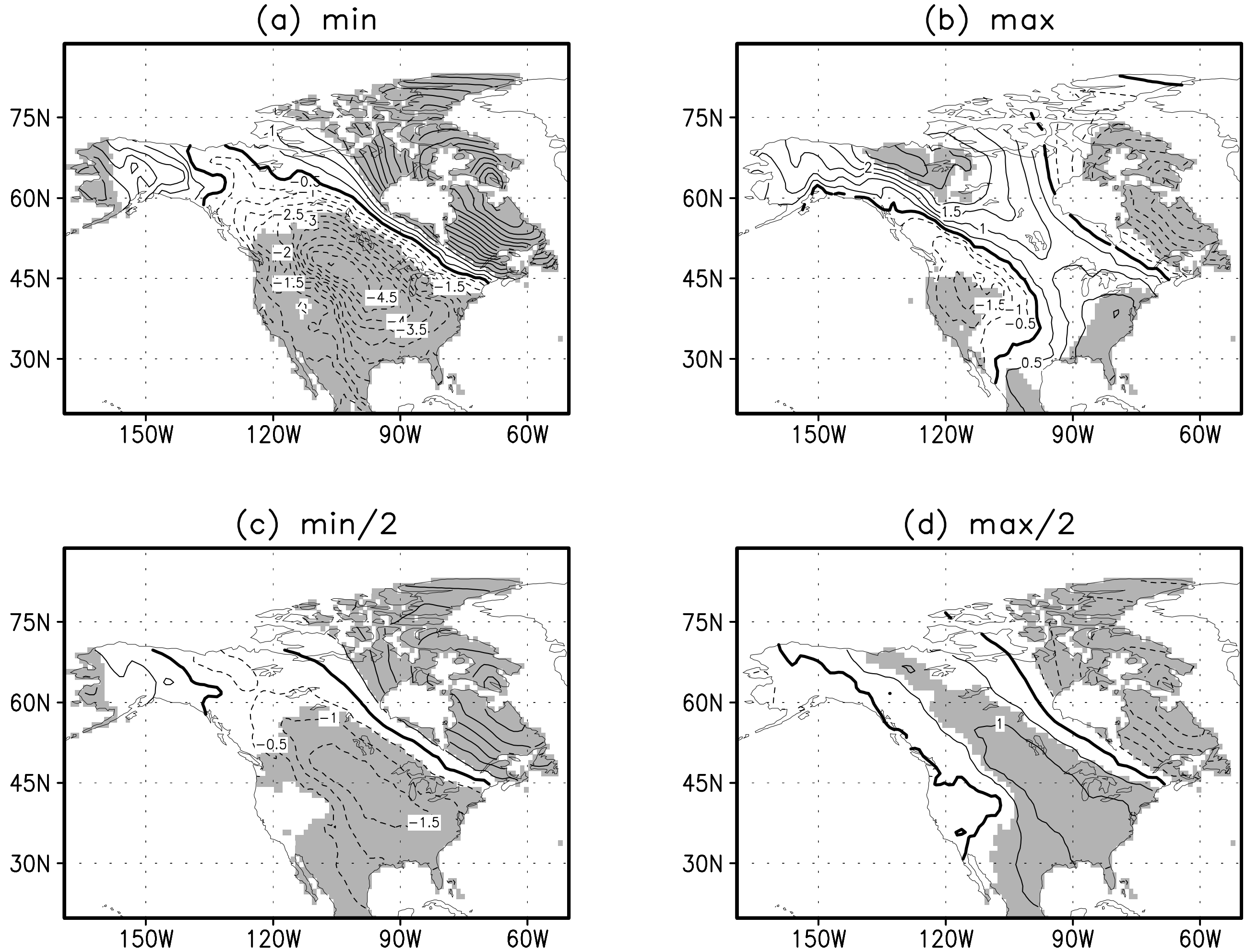

Figure 7: As in Fig. 5, but for the SAT anomalies. The contour interval is 0.5°C.

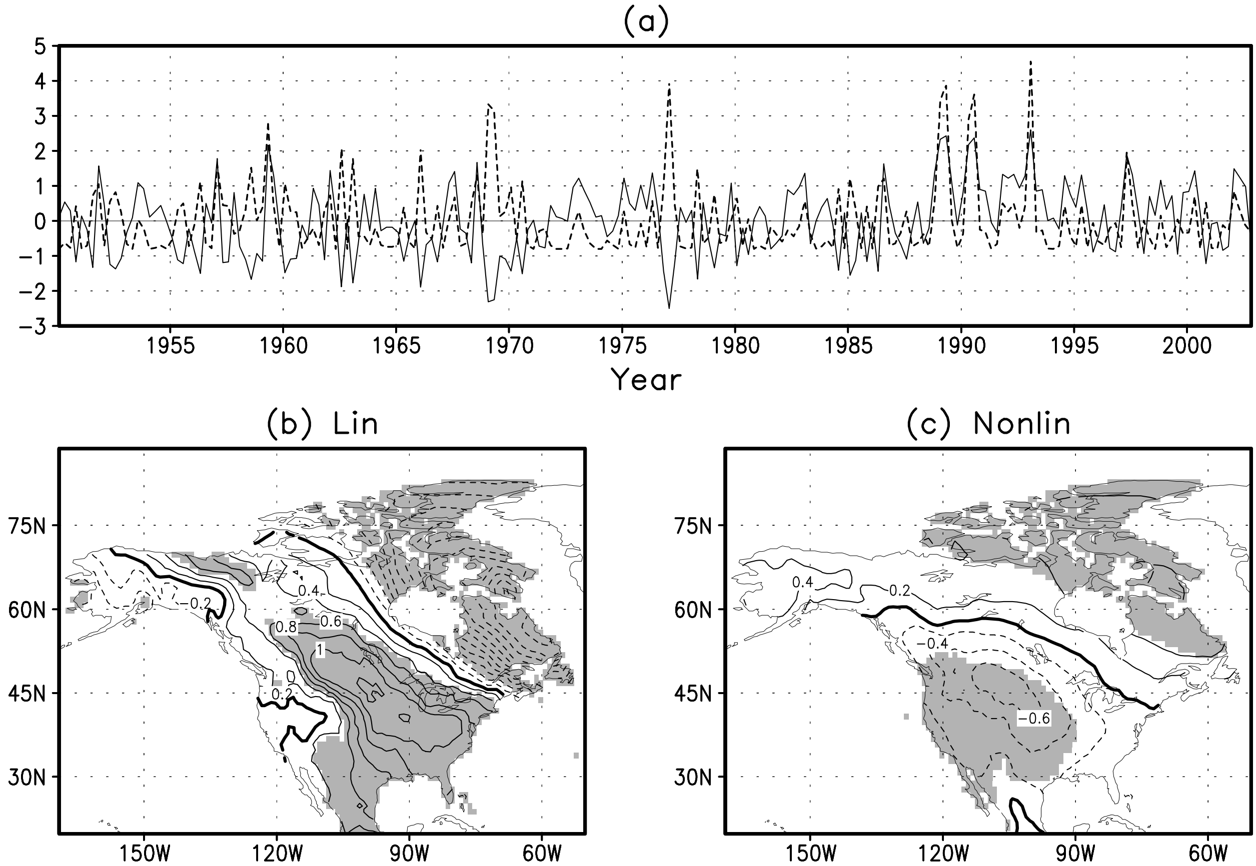

Figure 8: As in Fig. 6, but for the SAT anomalies. The contour interval is 0.2°C in panels (b) and (c).

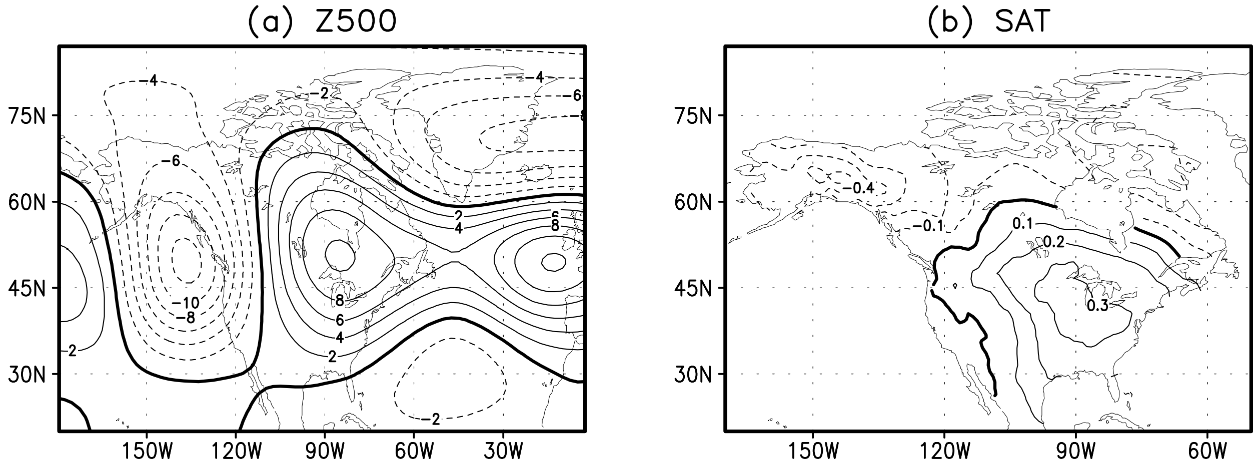

Figure 9: The nonlinear anomaly patterns of (a) Z500 and (b) SAT associated with one S.D. ENSO SST index. The contour interval is 2m for the Z500 field, and 0.2°C for the SAT field (reproduced from Wu and Hsieh (2004) and Wu et al. (2005) respectively).

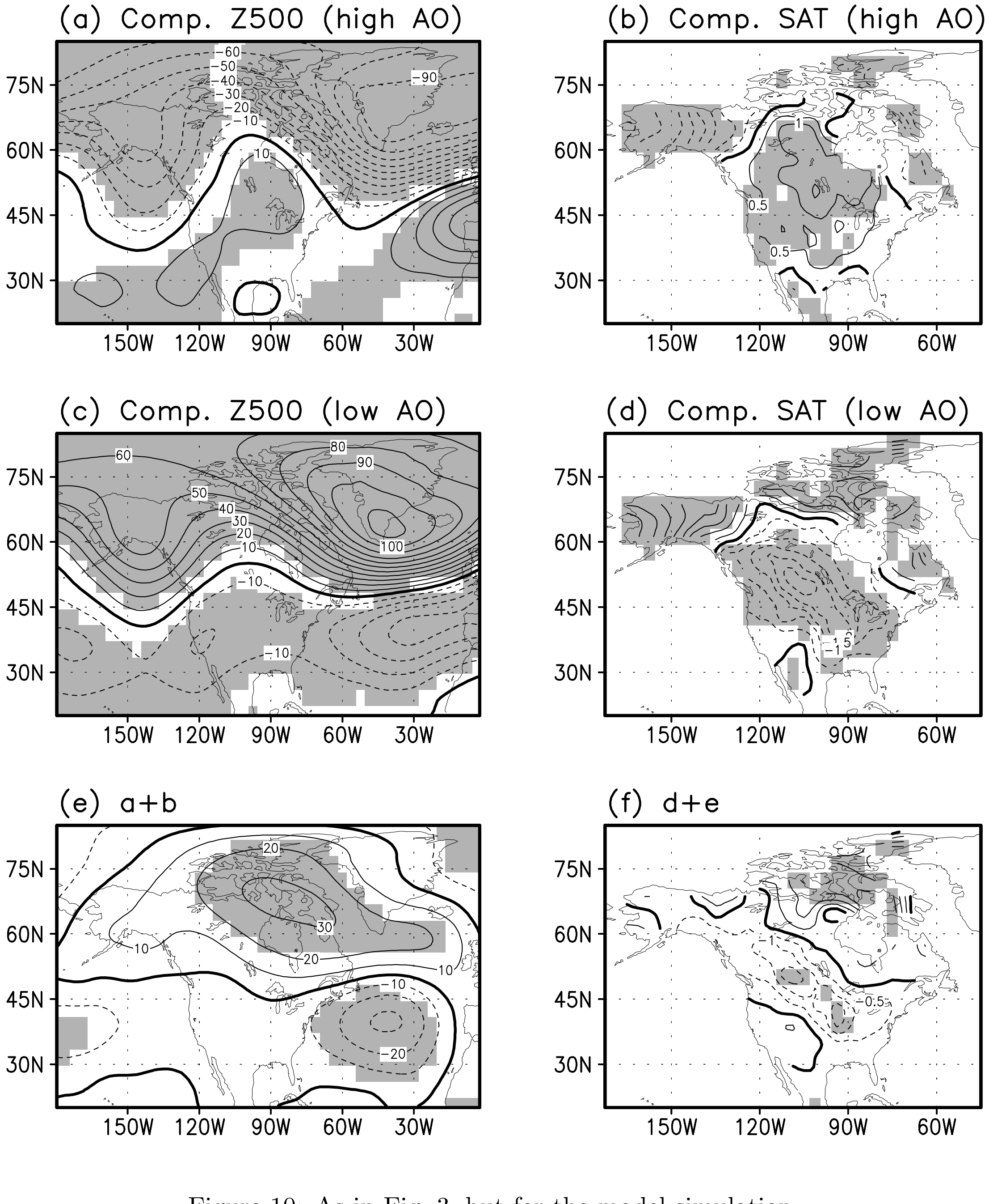

Figure 10: As in Fig. 3, but for the model simulation.

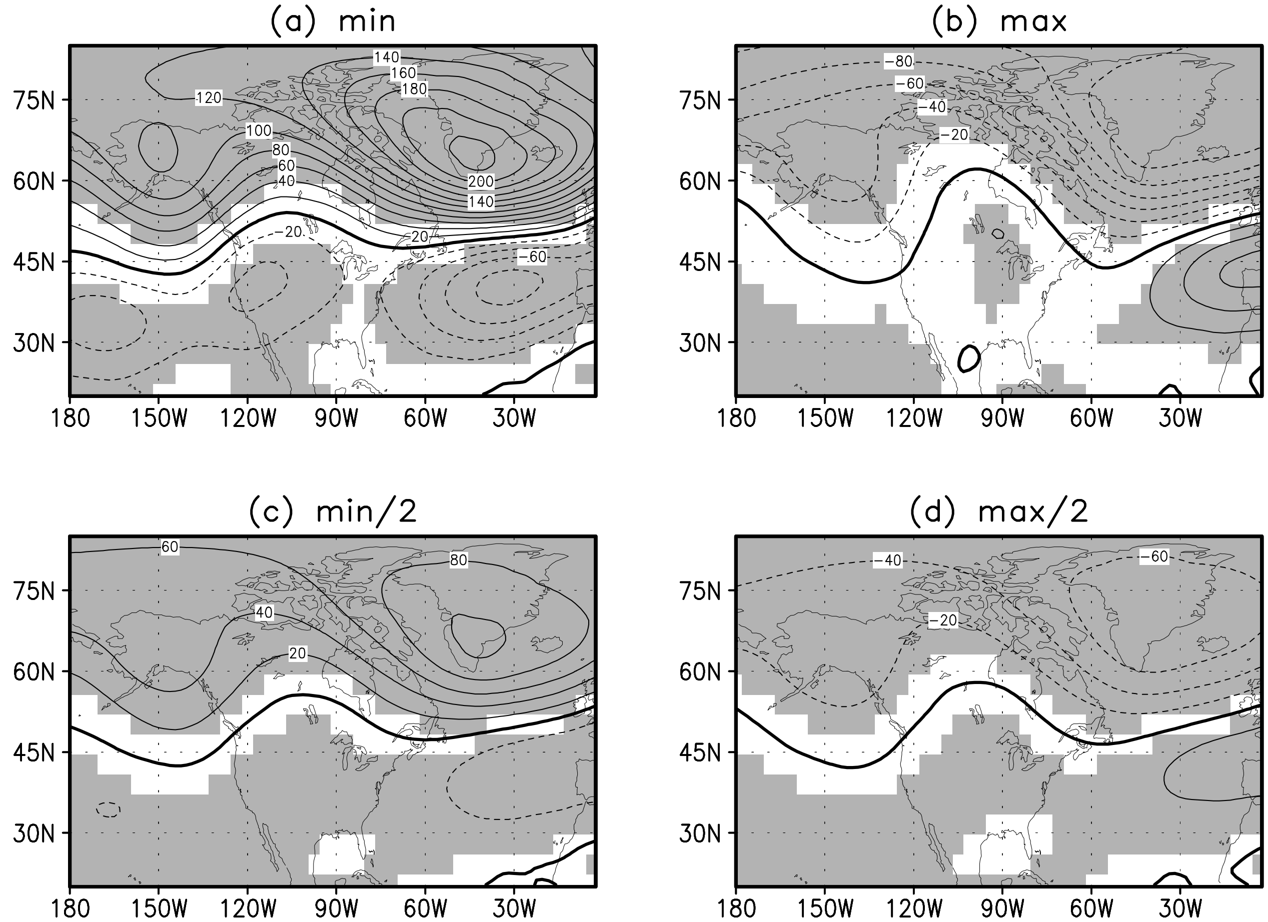

Figure 11: As in Fig. 5, but for the model Z500 anomalies.

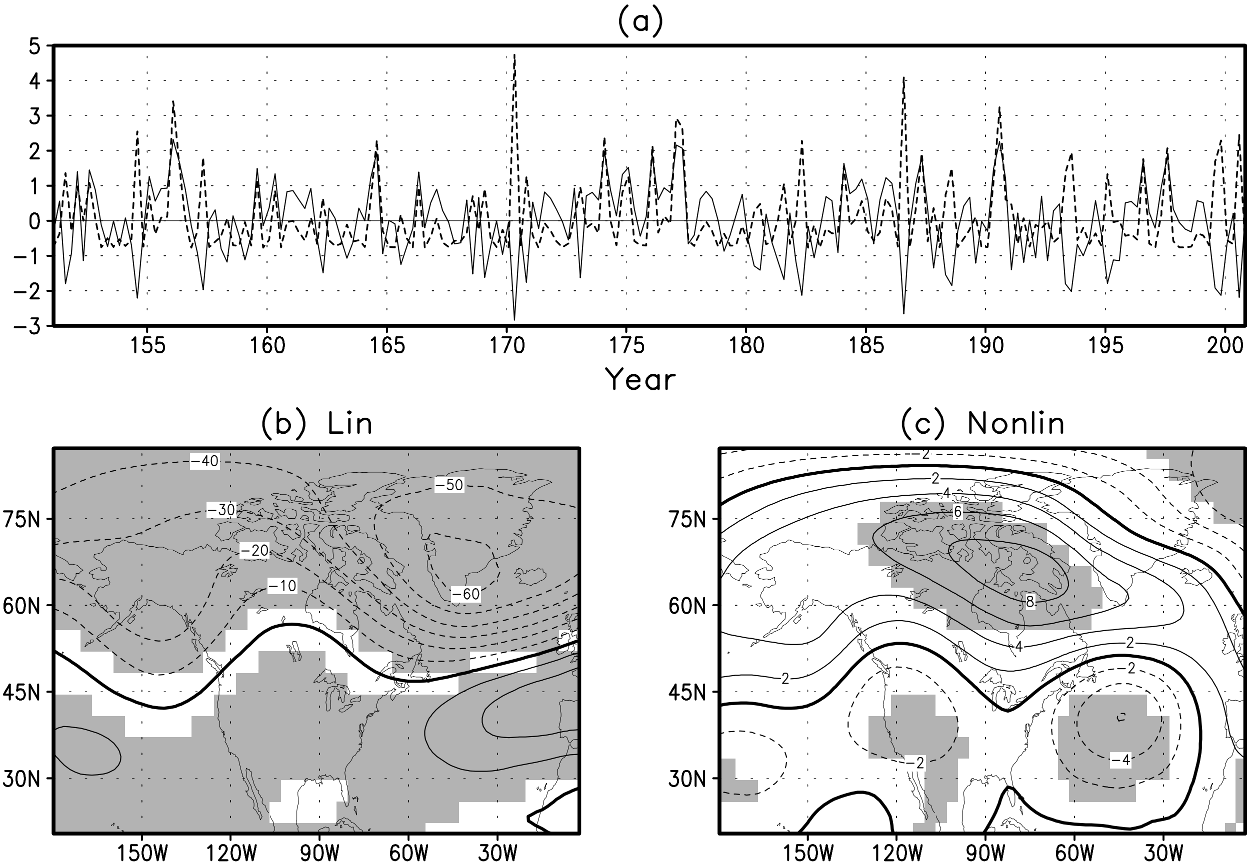

Figure 12: As in Fig. 6, but for the model Z500 anomalies.

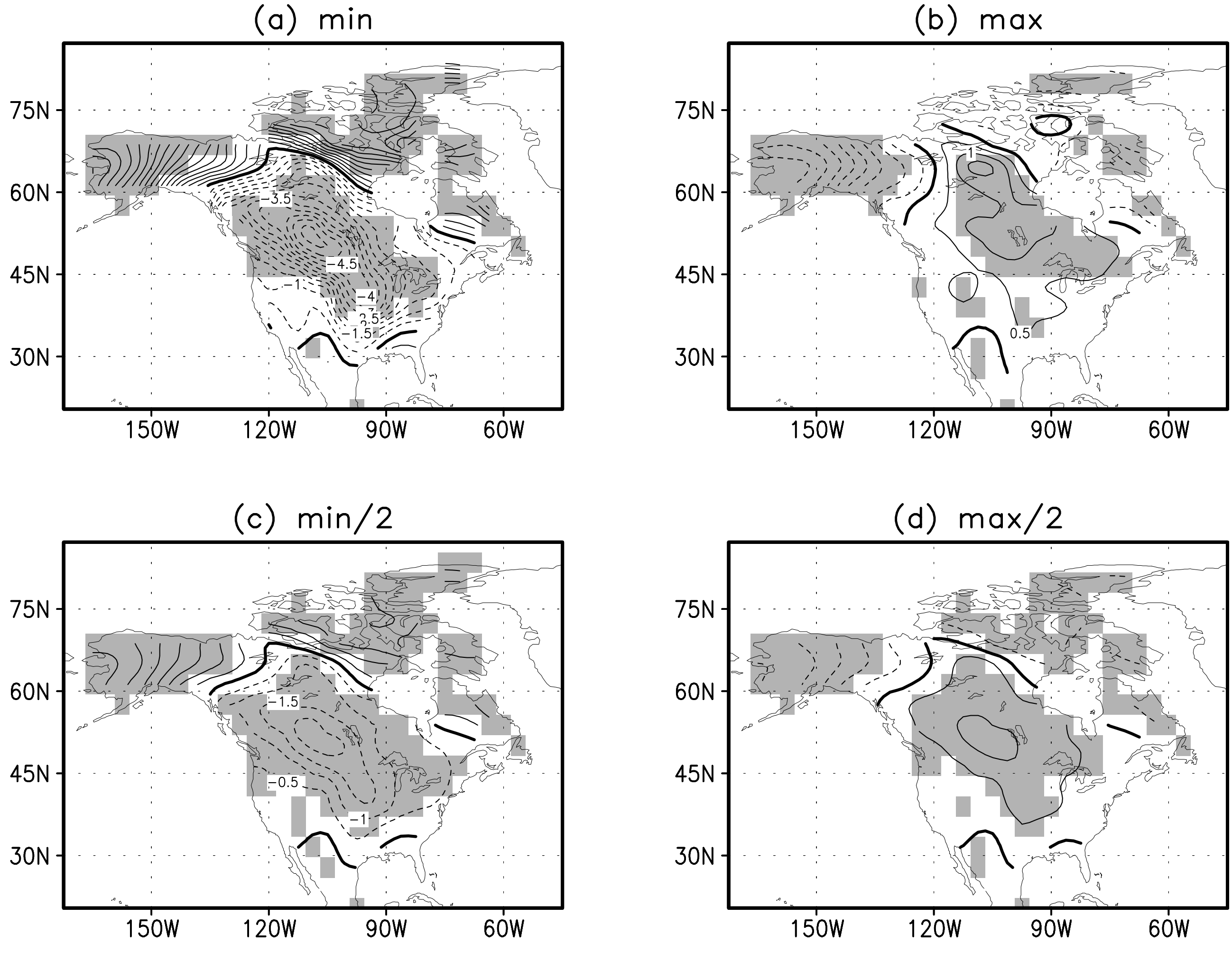

Figure 13: As in Fig. 7, but for the model SAT anomalies.

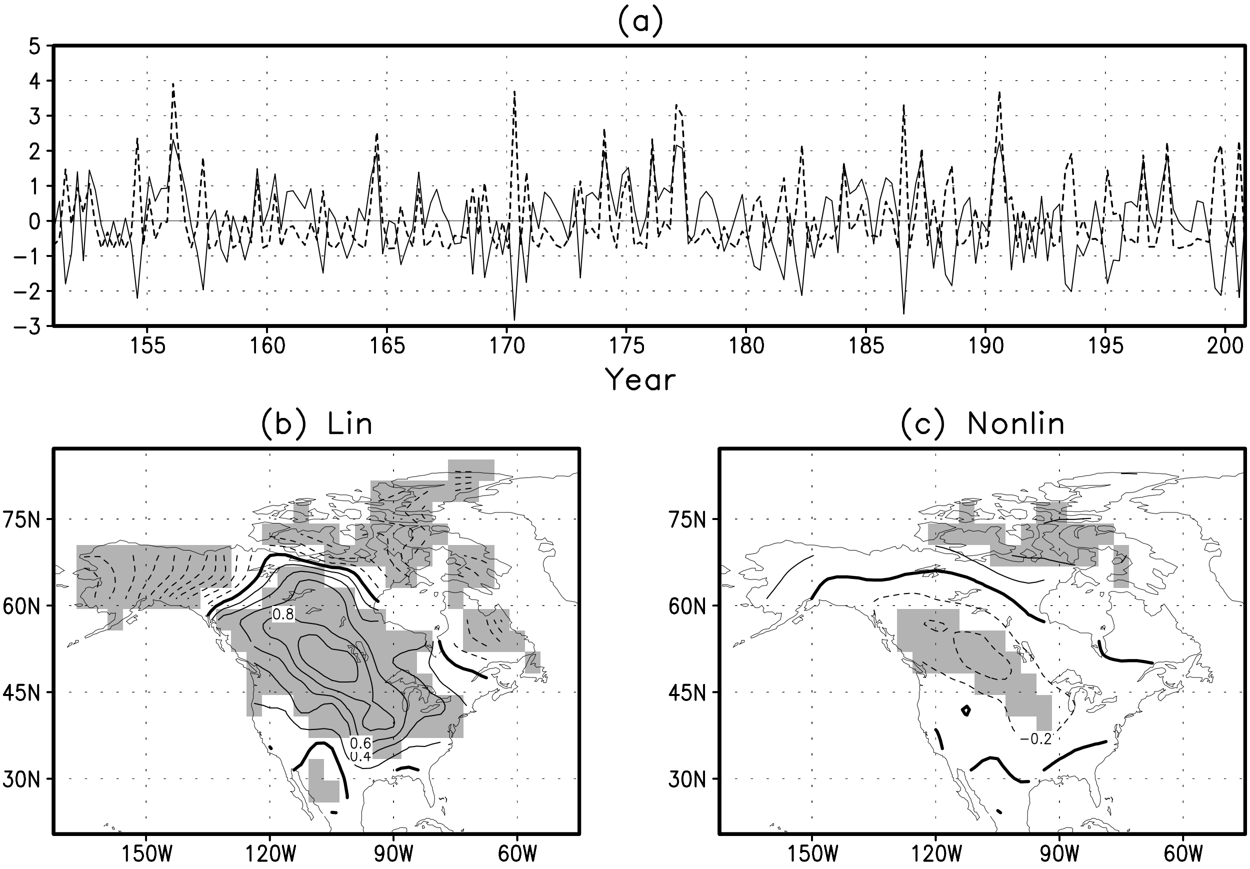

Figure 14: As in Fig. 8, but for the model SAT anomalies.